Environ. Sci. Technol. **2001**, *35,* 3823−3829

Seasonal Fluctuations in Zinc Speciation within a Contaminated Wetland

B. C. BOSTICK,*,† C. M. HANSEL,† M. J. LA FORCE,†,‡ AND S. FENDORF†

Department of Geological and Environmental Sciences, Stanford University, Stanford, California 94305-2155, and Department of Geological Sciences, San Francisco State University, San Francisco, California 94132-4163

The cycling of common sorbents such as metal (hydr)-oxides, carbonates, and sulfides in redox-active environments influences the partitioning of associated trace elements such as zinc. Consequently, fluctuations in redox status may in part determine the availability and mobility of Zn and other trace elements. This research examines changes in Zn speciation in a contaminated wetland soil that undergoes seasonal flooding. X-ray absorption spectroscopy (XAS) was employed to identify and quantify Zn species from soil cores collected over a 1-year cycle as a function of water depth, location, and soil depth. Zinc associated with (hydr)oxide phases in dry, oxidized soils and with sulfides and carbonates in flooded systems. An increase in water level was accompanied by a reversible change in Zn fractionation toward ZnS and $ZnCO_3$. However, a small, recalcitrant fraction of Zn associated with (hydr)oxides remained even when the soils were exposed to highly reducing conditions. Water depth and redox potential were the most important factors in determining Zn speciation, although spatial variation was also important. These data indicate that zinc sorption is a dynamic process influenced by environmental changes.

Introduction

Zinc is a ubiquitous contaminant that imposes a hazard to a host of plants and animals—many aquatic organisms are particularly sensitive to this element. Although it is not a redox active species within soil or aquatic environments, oxidation and reduction reactions may nevertheless affect zinc partitioning. Retention of zinc as well as other redox-stable cations such as cadmium can be modified by changes in substrate chemistry. Zinc sorbs strongly to iron (*1*, *2*) and manganese (hydr)oxides (*3*−*5*) in aerated systems and to sulfide (*6*, *7*) and carbonate (*8*−*10*) phases in anoxic environments. Thus, changes in redox status may shift Zn partitioning. For example, reductive dissolution of iron and manganese (hydr)oxides under suboxic conditions releases Zn into the aqueous phase; persistence of sub- or anoxic conditions may then lead to a repartitioning of Zn into sulfide or carbonate solids. However, slow transformation rates and fluctuation in conditions may alter these predicted phase changes.

* Corresponding author phone: (650)723-4152; fax: (650)725-0979; e-mail: bbostick@stanford.edu.

† Stanford University.

‡ San Francisco State University.

An appreciation of transformation rates of zinc partitioning is needed to predict its behavior and risk within natural environments. Model laboratory studies provide descriptions of zinc adsorption on an array of environmental solids and the solubility of neat compounds. Extending these results to natural environments provides a basis for describing zinc partitioning. However, zinc dynamics in redox active environments cannot be predicted with such information because changes in substrate have yet to be accounted for in the model systems. Thus, zinc speciation and partitioning within natural, dynamic environments needs to be examined further. Unfortunately, the complexity of natural systems is not easily dealt with when determining Zn speciation. Selective extractions have been used to empirically define mineral-associated fractions (e.g., refs *11* and *12*). While selective extractions provide a useful starting point to study Zn, or other trace element, partitioning, more direct means of analysis may provide additional and important information.

X-ray absorption spectroscopy (XAS) is an attractive method of determining the local structure of trace metals in situ and nondestructively within soil (*13*−*16*). Models of Zn sorption (*17*, *18*) as well as other divalent cations (e.g., ref *19*) have been refined with XAS; they have chronicled the importance of discrete Zn solids such as Zn hydroxides and sulfides.

In this study, XAS was used to determine changes in Zn partitioning within a seasonally saturated, mining-impacted wetland. A quantitative method was developed to determine the fractions of zinc oxide, zinc sorbed on iron (hydr)oxides, zinc sulfides, and zinc carbonates in the soil. Zinc speciation was correlated to soil redox status and the depth of the overlying water column. Response to the seasonal appearance of an overlying water column was also examined to determine the extent of kinetic control on Zn speciation.

Experimental Section

Sample Collection and Handling. Wetland soil samples were collected from a contaminated riparian wetland near the Coeur d'Alene River in northern Idaho (*20*). Three principal sites were chosen for detailed study that ranged from nearly dry to submerged throughout the year. Duplicate cores were taken at each site periodically using a 3.0 cm diameter piston-coring device; additional cores were taken from other wetland locations. Cores were stored upright at 4 °C and kept under nitrogen after sampling to minimize sample mixing and sample oxidation (*21*). Once in the laboratory, the cores were sectioned into 0−5 cm and 5−10 cm depths in an N_2-purged glovebox and homogenized. These wet soil pastes were mounted in 3 × 5 × 40 mm acrylic sample holders, sealed with Kapton film to prevent oxidation and moisture loss, and analyzed by XAS. Soil cores were collected and prepared immediately prior to analysis and kept refrigerated to minimize transformations during storage and sample collection. Neither Fe nor Mn oxidation state transformations were detected using XAS during sample handling. Sample pH and E_h were measured for the intact cores where possible using standard electrodes immediately following extraction.

EXAFS Spectroscopy. EXAFS spectra were collected at the Stanford Synchrotron Radiation Laboratory (SSRL) on beamlines 4−2 and 4−3. The storage ring operated at an energy of 3.0 GeV and at current between 50 and 100 mA. Spectra were collected about the Zn K-edge (−200 to +1000 eV) using a Si(220) double-crystal monochromator with an unfocused beam detuned approximately 50% to reject higher-order harmonic frequencies. Incident and transmitted intensities were measured with 15 cm N_2-filled ionization

10.1021/es010549d CCC: $20.00
Published on Web 08/24/2001

TABLE 1. Selected Characteristics of the Wetland Soils Used in This Study

sampling date	pH	org matter percent[a]	Fe		Mn		mineralogy[d]
			HCl,[b] mg kg^{-1}	HH,[c] mg kg^{-1}	HCl,[b] mg kg^{-1}	HH,[c] mg kg^{-1}	
Dec 1997	6.0	10.2	34300 ± 1170	5420 ± 456	278 ± 14	426 ± 43	quartz (Q), feldspar (F), muscovite (M), pyrite (P)
June 1998	6.2	11.3	24675 ± 813	1820 ± 135	229 ± 31	123 ± 23	Q, F, M, P

[a] Determined using loss on ignition. [b] Extracted using HCl, which targets both noncrystalline oxide and acid volatile sulfide phases. [c] Extracted using hydroxylamine hydrochloride, which targets crystalline oxide phases. [d] Silicates were analyzed by X-ray diffraction of the bulk soil, with pyrite identified by scanning electron microscopy.

chambers; sample fluorescence was monitored with a multielement Ge detector (*22*) oriented 45 degrees off the sample and orthogonal to the incident radiation. Internal energy calibration of each spectrum was achieved with a Zn foil placed between the second and third ionization chambers; its inflection edge was set to 11 659 eV.

Data Analysis. XAS data were analyzed using EXAFSPAK (Graham George, SSRL). The background was subtracted from averaged spectra using a polynomial fit and their absorbance was normalized to unity. A cubic spline function was fit to four points in the spectrum that followed the envelope of the decaying EXAFS, or χ(k), spectrum, and the photon energy was converted to wavevectors using an E_o of 11 685 eV. The χ(k) spectrum was then weighted by k^3 in order to provide an equal amplitude throughout the entire k-range. The k-weighted χ(k) spectrum was Fourier transformed without smoothing to produce a radial structure function (RSF) using a k-range of approximately 3−12 Å^{-1}. The RSF was then sectioned to isolate the contributions of each atomic shell, and these individual shells back transformed into isolated χ(k) functions. The local coordination environment of Zn, including the type (Z), coordination number (CN), distance (R), and the Debye−Waller factor (σ^2) of neighboring atoms, was then determined by fitting the experimental spectrum using theoretical phase and amplitude functions (*23*, *24*) and an amplitude correction factor of 0.9. Known coordination numbers and interatomic distances were used for reference compounds. Final fits used raw, unsmoothed $k^3\chi$(k) data. Accuracy of the fits was estimated using the χ^2 statistic, for which smaller values correspond with the best fits. All fits had χ^2 values of about 2.5 with unsmoothed χ(k) spectra and approximately 0.7 with smoothed data. By comparison with model compounds, the interatomic distances were accurate within 0.02 Å and the coordination number within 20% for the first shell with less accuracy for more distant shells. Elements of different atomic number ($\Delta Z > 2$) can be distinguished based on phase and amplitude functions.

Several Zn standards, including ZnS, ZnO, and $ZnCO_3$, were analyzed for comparison with natural samples and to validate the theoretical parameters used in XAS fitting. In addition, Zn-substituted $CaCO_3$ was analyzed to determine whether this solid solution could be differentiated from $ZnCO_3$. Zn-substituted calcite was synthesized according to the procedure of Reddy and Nancollas (*25*), replacing 0.01 mole fraction of the calcium with Zn.

Selective Sequential Extraction. Selective sequential extractions are commonly used to provide information about the chemical speciation of associated trace metals (*11*, *12*). Accordingly, sequential extractions were used to identify Zn associations in selected samples to confirm speciation determined by XAS. These samples (12 replicates each) were extracted according to the procedure of La Force et al. (*20*). Briefly, a 1 M $MgCl_2$ solution reacted with 2 g solids for 1 h was used to remove the soluble Zn species. Second, the carbonate phases were extracted with 1 M sodium acetate/acetic acid for 5 h. The sample was then split for determination of noncrystalline oxides and acid-volatile sulfides (AVS) fractions. Noncrystalline (hydr)oxides and AVS were extracted with 1 M HCl in one subsample, and noncrystalline (hydr)-oxides were extracted with ammonium oxalate (AOD) in the dark. Zn associated with AVS was then determined by the difference between the HCl-extractable and AOD-extractable fractions. Sodium hypochlorite was reacted with residual solids from the HCl extraction at 95 °C to remove organic matter-associated Zn. A heated hydroxylamine/acetic acid extraction dissolved the crystalline (hydro)oxides. Residual silicates were removed by reflux with 10 M HF. Finally, pyritic sulfides were extracted using nitric acid. It should be noted that sequential extractions depend on the specific and complete extraction of a target phase and are operationally defined mineralogical fractions. Despite limitations caused by inefficient or nonspecific extractions, selective sequential extractions provide a useful, albeit approximate, method of quantifying Zn speciation in soils.

Results and Discussion

Site Characteristics. Wetland soil samples were composed of a mixture of quartz and feldspars with some residual mine tailings minerals, including pyrite (Table 1). The total Zn content of the soils was approximately 1900 mg kg^{-1} (determined by total digestion). Additionally, secondary Fe and Mn phase concentrations vary with site and season (*20*). Water levels varied substantially during the year within the wetland. During the summer, only a portion of the wetland was submerged; however, standing water up to 150 cm deep covered the wetland during winter and spring. Temperature oscillation accompanied this water level variation, with the temperature of the sediment−water interface ranging from 20 °C in summer to 6 °C in winter. The pH ranged from 5.6 to 6.6, generally being most acidic in dry samples and most alkaline under standing water. The redox potential (E_h) was not determined for dry samples; wet samples had an E_h of about +200 mV when soils were saturated but not ponded and as low as −200 mV when ponded (>100 cm water column depth), although E_h was variable for any given water depth.

Model Compounds. The standard compounds of Zn used in this study contain significant variation in first-shell coordination environment that is reflected in the bond lengths and coordination numbers of the XAS data (Table 1). In ZnS, Zn is coordinated to four sulfur atoms at a distance of 2.33 Å, significantly longer than Zn−O bond lengths that range between 1.96 Å in ZnO and Fe_2ZnO_4 (tetrahedral Zn coordination) to 2.11 Å in $ZnCO_3$ (octahedral Zn coordination). Organically bound Zn species have a similar first coordination shell to inorganic species (e.g., refs *26* and *27*), and thus second-nearest neighbor information is required to discriminate between them. Zinc (hydr)oxides exhibit significant second-shell contributions due to the effective scattering of the Zn atom, while organically complexed Zn exhibits only weak contributions in the second-shell. Thus, each Zn species could be identified by their unique set of interatomic distances.

Identification of Principal Zn Species in Soils. These wetland soils undergo seasonal redox transformations typical of many palustrine emergent wetlands that may alter Zn

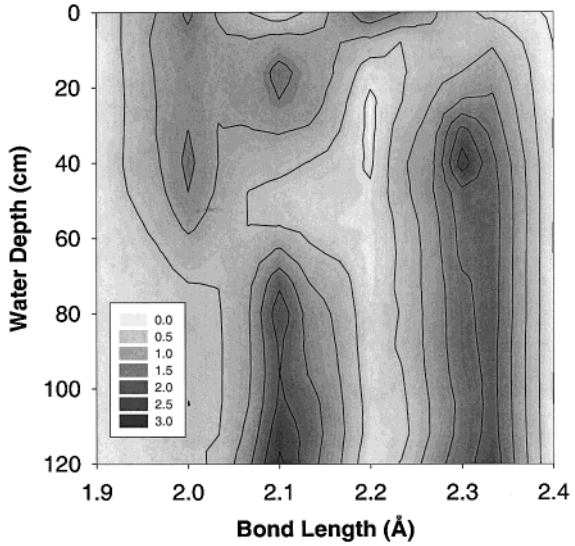

FIGURE 1. Changes in the first-shell Zn coordination number and bond length as a function of water depth. Each point is the average coordination number of data from at least two samples of similar water depth regardless of position in the wetland or sampling date. Three principal coordination environments were found, Zn−O at distances of approximately 2.0 and 2.1 Å, and Zn−S bonds at 2.33 Å.

speciation. In fall, the soil in much of the wetland is dry and warm, leading to the effective oxidation of the material. Snow and rain saturates the soil in winter and spring; coupled with biological activity this leads to reducing conditions. Several Zn compounds are likely present under these environmental conditions; Zn solids such as ZnO, ZnS, and $ZnCO_3$ are all possible species within the wetland. The hydroxide and oxide phases are most stable under oxic conditions common in well-drained soils, while the sulfide and carbonate solids are most stable under anoxic conditions where sulfur is reduced and gas exchange with the atmosphere is impeded. Additionally, Zn may adsorb on hydroxides or organic matter or be incorporated into oxides or carbonates. The presence of Zn-containing phases were evaluated by comparing the bond distances found in the soil samples with those of the model compounds (Table 2).

Three distinct coordination environments in the first shell (Figure 1) dominate the local structure of Zn in the wetland soils, Zn−O shells at 2.0 and 2.1 Å and a Zn−S shell at 2.33 Å. Samples with a 2.0 Å Zn−O distance, *d*(Zn−O), also contained a second shell feature attributed to Zn−Zn or Zn−Fe at 3.1 Å. As water depth increased to 50 cm, the coordination number to oxygen at this short distance decreased from approximately 1.5 to 0, indicating that the fraction of this species was greatest under oxic conditions and decreased with the onset of reduction. Such bond distances are consistent with ZnO (Table 2 (*28*)). Adsorbed Zn species exhibit a variable structure that may also contain similar interatomic distances and thus cannot be ruled out based on this spectral data (*18*). Other phases that have similar *d*(Zn−O), such as Zn_2SiO_4, $Zn_5(OH)_6(CO_3)_2$, and $ZnFe_2O_4$, can be disregarded based on their distinct second shell environments. The Zn_2SiO_4 lacks an Fe or Zn second shell entirely (*29*), while $Zn_5(OH)_6(CO_3)_2$ and $ZnFe_2O_4$ both have *d*(Zn−Zn/Fe) significantly longer than observed in these samples (Table 2 (*30, 31*)).

Under flooded conditions, a Zn−S shell at 2.33 Å is noted that is indicative of ZnS (Figure 1, Table 2). Zinc sulfide second-shells, with a *d*(Zn−Zn) of 3.8 Å, are also observed in some of the samples (*32*). Both ZnS polymorphs (wurtzite and sphalerite) have similar local structures; thus, we are unable to distinguish between them using these data. Zinc sulfide is also an important Zn phase in other mine-impacted fluvial (*18*) and estuarine sediments (*33*). Sulfide minerals commonly form in anoxic, sulfidic environment; thus, it is not surprising that ZnS was observed. Zinc may also be complexed by other S-containing ligands such as proteins and organic sulfides (*34*). However, the organic complexes lack second-shell Zn spectral features and thus are not consistent with our analyses of the unknowns. Additionally, insufficient organic thiols are present in these soils to explain a large fraction of Zn sorption. These wetland soils contain approximately 10% organic matter (*35*), which typically contains a small quantity of S. Much of this organic sulfur is also oxidized sufficiently to prevent direct coupling of Zn to S (*36*, *37*).

In flooded soil systems, the average CN of the 2.1 Å Zn−O shell was approximately 2.5, decreasing to 0 at a water depth of ~50 cm, and then increasing to 3 at water depths greater than 75 cm (Figure 1). The bimodal distribution suggests the presence of two distinct Zn species with similar first-shell Zn−O shells. To test this premise, we examined their second coordination sphere (Figure 2). The Zn local structure in soils under little or no standing water contained second-shells of about 1 Zn or Fe at a distance of 3.1 Å. The presence of an iron shell with low CN coupled with the short d(Zn−Fe/Zn) suggests that Zn in this system is adsorbed to an iron (hydr)oxide or within a hydroxide (*38*). Zn sorbed on hydrous ferric oxide, commonly encountered in oxic soils, has a similar coordination environment ((*18*) Table 2).

In contrast, samples with a *d*(Zn−O) of 2.1 Å contained a *d*(Zn−Fe/Zn) of 3.68−3.78 Å when under >75 cm water (Figure 2). These bond lengths correspond with smithsonite, $ZnCO_3$ (*39*). Evidence of Zn-substituted calcite was not present—the *d*(Zn−Fe/Zn) of about 3.7 Å observed is shorter and distinct from the 4.02 Å *d*(Zn−Ca) found in Zn-substituted calcite (Table 1 (*40*)). Typically, Zn sorption on calcite results in the replacement of Ca atoms at the surface and the subsequent formation of discrete $ZnCO_3$ domains (*9*, *10*, *41*). $ZnCO_3$ also may have formed directly through precipitation with bicarbonate.

Quantification Method. The XAS data suggests that four primary Zn species are identifiable within this wetland system: ZnO, $ZnCO_3$, Zn sorbed to a (hydr)oxide, and ZnS, although others may be present. Multiple methods have been developed to determine the fractions of various species in complex mixtures, including approaches that use coordination numbers (e.g. refs *42* and *43*) and linear combinations of EXAFS and XANES spectra (e.g. refs *44* and *45*). We determine the fractions of Zn species using the first-shell coordination numbers. This method can determine species with different crystallinity and structures. In contrast, linear combinations of EXAFS spectra are largely influenced by small differences in structure. Furthermore, the accuracy of the shell fitting approach does not require a comprehensive spectral library; shell fitting depends only on knowledge of the local structural environment.

The first-shell coordination numbers were used to calculate the fractions of each Zn species. The fraction (χ) of the *i*th species was determined with the ratio of the fit coordination number (CN_i) to the model compound (CN_s)

$$\chi_i = \frac{CN_i}{CN_s} x \frac{1}{N} \tag{1}$$

where *N* is a normalization constant used to make all fractions add to unity.

$$N = \sum_{i=1}^{n} \frac{CN_i}{CN_s} = \frac{CN_{ZnO}}{4} + \frac{CN_{ZnCO_3}}{6} + \frac{CN_{Zn(hydr)oxide}}{4} + \frac{CN_{ZnS}}{4} \tag{2}$$

TABLE 2. Local Structures of Various Zn Model Compounds Based on Crystallography (XTL) and Determined with X-ray Absorption Spectroscopy (XAS)

		CN		distance (Å)		source	
compound	atom	XTL	XAS	XTL	XAS $\pm \sigma^{-2}$ in Å^2	XTL	XAS
ZnO	Zn−O	4	5.03	1.96	2.01 ± 0.004	Abrahams and Bernstein, 1969	this work
	Zn−Zn	12	10.6	3.21	3.19 ± 0.006		
$Zn(OH)_2$	Zn−O	6	6	1.87−2.06	1.95−2.08	Christiansen, 1969	O'Day et al., 1998
	Zn−Zn	2,2		3.29, 3.50			
$ZnCO_3$	Zn−O	6	5.87	2.11	2.11 ± 0.005	Effenberger et al., 1981	this work
	Zn−C	6	*b*	2.98	*b*		
	Zn−Zn	6	6.12	3.67	3.69 ± 0.004		
Zn_2SiO_4	Zn−O	4	5.03	1.96	2.01 ± 0.004	Hang et al., 1970	*b*
	Zn−Si	4	10.6	3.1−3.3	3.19 ± 0.006		
Fe_2ZnO_4	Zn−O	4	3.55	1.99	1.98	Koenig and Chol, 1968	this work
	Zn−Fe/Zn	18, 4	15.6, 5.27	3.5, 3.65	3.51,3.66		
$Zn_5(OH)_6(CO_3)_2$	Zn−O	6	*b*	2.11	*b*	Ghose, 1964	*b*
	Zn−C	2	*b*	3.08	*b*		
	Zn−Zn	2,6	*b*	3.18, 3.55	*b*		
Zn in $CaCO_3$	Zn−O	6[a]	6.46	2.36[c]	2.11 ± 0.003	Effenberger et al., 1981	this work; Reeder et al., 1999
					2.14 ± 0.003		
(0.01 mole fraction)	Zn−C	6[a]	*b*	3.21[c]	*b*		
	Zn−Ca	6[a]	6.57	4.04[c]	4.02 ± 0.003		
					3.94 ± 0.003		
Zn-humate	Zn−O	*b*	6	*b*	2.08	*b*	Xia et al., 1997
	Zn−C	*b*	1	*b*	2.78	*b*	
Zn-thiolate in protein	Zn−S	*b*	4	*b*	2.30	*b*	Clark-Baldwin et al., 1998
Zn-histidine	Zn−O	*b*	1.1	*b*	2.08	*b*	Salt et al., 1999
	Zn−N	*b*	3.8	*b*	2.23	*b*	
Zn on HFO	Zn−O	*b*	2	*b*	1.92 ± 0.0042	*b*	O'Day et al., 1998
	Zn−O		2		2.04 ± 0.003		
	Zn−Zn	*b*	1.2	*b*	3.54 ± 0.004	*b*	
	Zn−Fe	*b*	0.7	*b*	3.12 ± 0.004	*b*	
ZnS	Zn−S	4	3.83	2.34	2.35 ± 0.005	Kisi and Elcombe, 1989	this work
	Zn−Zn	12	8.06	3.82	3.85 ± 0.008		

[a] Fixed during fitting. [b] Not available. [c] Based on calcite crystallography.

The value of N was typically near one, although it varied from 0.65 to 1.3. Most variation in N could be attributed to different values of σ^2 used in the EXAFS structural optimization; normalization reduced the effect of variation in the Debye−Waller factor.

This fitting method involves several simplifications. The $ZnCO_3$ and Zn sorbed on (hydr)oxides fractions could not be quantified concurrently because the same Zn−O shell was used for quantifying both species. However, they could be differentiated based on environmental conditions. Under dry or shallow water levels (oxic conditions), EXAFS data indicate that Zn is sorbed to (hydr)oxide phases. Therefore, all Zn with a 2.1 Å Zn−O bond length was assumed to be present as Zn sorbed on (hydr)oxide for water depths less than 50 cm. At water depths greater than 50 cm, Zn coordinated to O at 2.1 Å was assumed to be $ZnCO_3$. While both phases may occur concurrently in some samples, the bimodal occurrence of the 2.1 Å Zn−O shell indicates that the two species are largely exclusive (Figure 1).

An additional simplification involved the combination of ZnO and Zn sorbed to (hydr)oxides into one fraction, the ZnO/sorbed fraction. Both ZnO and Zn sorbed to (hydr)-oxides are founds predominantly in oxic environments, and their similar first-shell coordination environments often cannot be effectively resolved using XAS spectroscopy due to their similar d(Zn−O) (Figure 3). Additionally, the fit distances of the ZnO fraction may be attributed in part to hydroxides (*18*). Finally, the errors associated with shell fitting caused by inaccurate coordination number should be

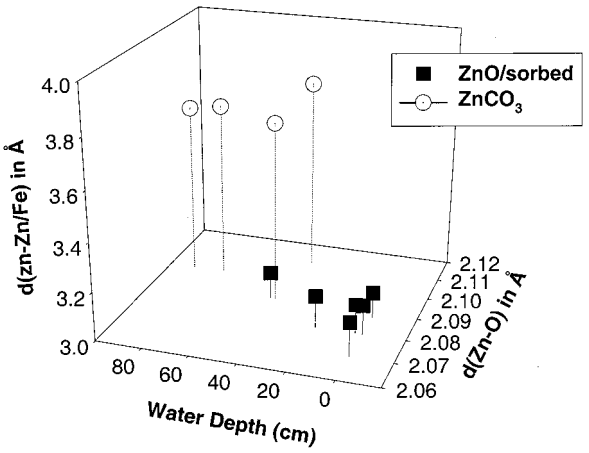

FIGURE 2. The second coordination sphere of Zn. For clarity, only data with Zn−O distances near 2.09 Å with distinguishable second-shells are included. At shallow water depths, second-shell data indicates that a (hydr)oxide phase is present, while a carbonate phase is present at higher water depths.

acknowledged. Despite these limitations, shell fitting provides a favorable method for Zn speciation.

Seasonal Variation in Zn Speciation. Seasonal effects on Zn speciation were evaluated by repeatedly analyzing soils from each of the three sites over 1 year. Figure 3 contains

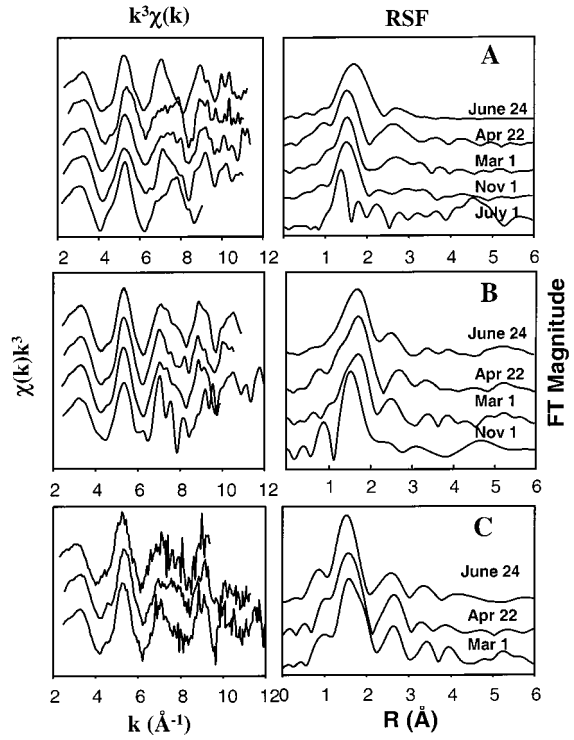

FIGURE 3. Weighted χ(k) spectra and RSF's of samples collected from (A) an aerated wetland location, (B) a shallow, ponded location (average water depth of 30 cm), and (C) a flooded region of the wetland (~50 cm water).

example weighted χ(k) spectra and RSFs for three locations within the wetland ranging from predominately dry to permanently flooded. Figure 4 shows the Zn fractions that are present in these samples as a function of collection time. In general, these spectra indicate a change in the first coordination sphere between the dry summer months and the wet winter and spring periods. The bond length of this shell typically increases as conditions shift from oxic to anoxic, indicating the gradual change in Zn fractionation toward more reduced phases such as carbonates or sulfides.

The driest location exhibited large shifts in Zn speciation; a small increase in water levels associated with spring flooding results in the conversion of the ZnO/sorbed fraction to the ZnS fraction (Figure 4A). Similar fluctuations in Zn species were detected in samples from a portion of the wetland typically covered by about 30 cm water (Figure 4B). At this site, a gradual increase in water level in winter was accompanied by a small increase in the ZnS fraction and a decrease in the ZnO/sorbed fraction. While sulfides formed the dominant Zn fraction at all sample dates, the June 24 sampling date exhibited an increase in (hydr)oxide associated Zn that correlates with a decrease in water depth during that period.

The largest changes in Zn speciation occurred in an area of the wetland covered by about 50 cm water (Figure 4C). The ZnO/sorbed fraction decreased markedly with an increase in water depth resulting from the spring runoff. Both ZnS and $ZnCO_3$ were present in appreciable quantities; however, the proportion of ZnS decreased, while $ZnCO_3$ content increased with water level during the spring. The decrease in the oxide-sorbed Zn is expected as conditions become more reduced; however, the relationship between the ZnS and $ZnCO_3$ fractions was not easily explained.

It is apparent that Zn fractionation responds readily to changes in environmental conditions. While thermodynamic considerations describe the conditions under which ZnO/

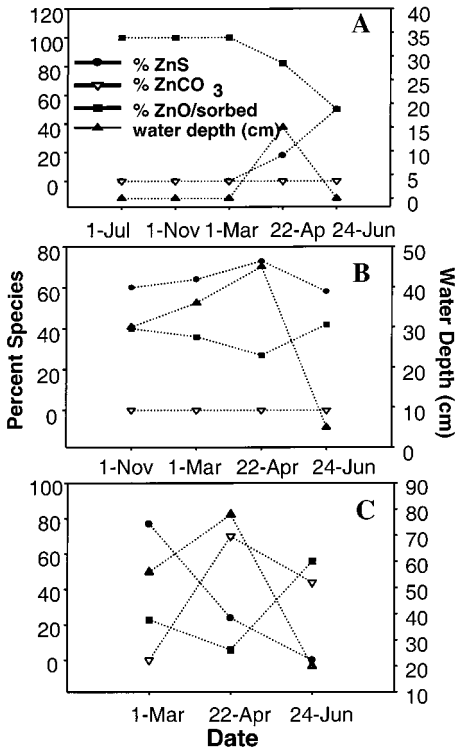

FIGURE 4. Zn fractionation and water depths for three wetland locations: (A) within an aerated wetland location, (B) within a shallow, ponded region (average water depth of 30 cm), and (C) in a flooded region (~50 cm water). These fractions are determined using the spectra that appear in Figure 3 for each site. In oxidized conditions, Zn is found in the ZnO or Zn sorbed on (hydr)oxide fractions. The fraction of ZnS and $ZnCO_3$ rises with water levels in spring.

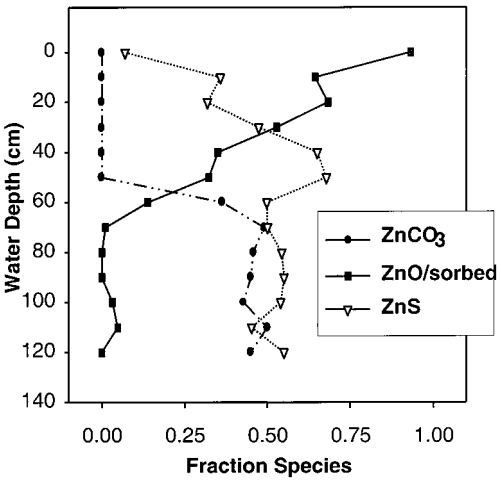

FIGURE 5. Zinc speciation as a function of water depth. Fractions for each depth are the average of all samples collected in the wetland with similar water depth, regardless of sampling date or sampling position. Sorption as ZnO or Zn sorbed to (hydr)oxide phases decreases as water depth increases to 50 cm, while the ZnS fraction increases rapidly to a maximum at approximately 50 cm water depths. Carbonate phases begin to appear at approximately 50 cm water depth.

sorbed, ZnS, and $ZnCO_3$ occur, the kinetics of these processes are not well understood. The majority of Zn solid phases are assumed to be kinetically stable due to their low solubility (*8*, *46*, *47*). For example, authigenic zinc sulfide found in oxic sediments from the Tri-State mining district undergoes

TABLE 3. Zn Fractionation and Water Depths for Selected Soil Core Sections.

sample water depth (cm)	core section (cm)	% ZnO	% sorbed Zn on hydroxide	% ZnS	% $ZnCO_3$
0	0−5	0 ± 0[a]	97 ± 2	3 ± 2	0 ± 0
0	5−10	0 ± 0	96 ± 2	4 ± 2	0 ± 0
36	0−5	0 ± 0	38 ± 2	62 ± 2	0 ± 0
36	5−10	0 ± 0y	36 ± 4	64 ± 4	0 ± 0
39	0−5	43 ± 2	0 ± 0	57 ± 3	0 ± 0
39	5−10	43 ± 5	0 ± 0	57 ± 5	0 ± 0
89	0−5	0	0	85	15
89	5−10	0	0	80	20
105	0−5	12	0	0	88
105	5−10	10	0	0	90

[a] Each value represents the average of duplicate cores ± the standard deviation. Where single values are given, only one core was analyzed.

incomplete oxidation (*18*, *48*). However, our results demonstrate that Zn speciation can respond rapidly to changes in redox status. ZnS in this system formed through secondary (authigenic) processes, while it was of primary origin in the Tri-State mining district (*18*, *48*).

Pure ZnO and $ZnCO_3$ are resistant to oxidation and reduction reactions because they do not contain species that undergo redox transformations. However, they do respond to changes in redox status. The rapid response of sorbed species to changes in environmental conditions has been documented in other flooded soils and sediments (*49*, *50*) and is often attributed to microbial transformations (*51*, *52*). Microbial processes may similarly influence changes in Zn speciation within this wetland, either through direct oxidation of ZnS or the indirect dissolution of oxide (such as Fe oxides) and carbonate phases.

Pure solid phases such as ZnO were found to dominate the speciation of Zn here and elsewhere (*18*). However, solutions were undersaturated with respect to pure ZnO in our studies. Isomorphous substitution lowers the solubility product significantly (*53*, *54*); Fe^{2+} and Mn^{2+} substitution may therefore explain the rapid conversion of Zn solids in response to environmental changes. Unfortunately, it is difficult to quantify the extent of substitution.

Comparison of XAS Quantitation and Selective Extraction. Selective sequential extractions are a traditional method determining trace metal associations in soils and sediments. Despite several caveats (e.g., refs *56*−*58*), these methods provide a means of corroborating the Zn partitioning found by XAS in these wetland samples. Additionally, they offer the opportunity to examine Zn partitioning in many phases that cannot be determined concurrently using XAS alone. Four principal Zn phases were identified with selective extractions: Zn associated with (1) noncrystalline oxides, (2) crystalline oxides, (3) carbonates, and (4) acid-volatile sulfides (Table 4). Importantly, these phases are similar to those identified using XAS, although extractions can differentiate somewhat between noncrystalline oxides and more crystalline forms. Sequential extractions also show the dynamic changes in Zn speciation throughout the seasons observed by XAS (Table 4). The fraction of Zn associated with (hydr)-oxides peaked during the summer, while Zn in carbonate fractions was highest in spring and early summer when water levels were greatest. Sulfide-associated Zn also increased with water depth for the shallow, ponded site, although this trend was not observed for the flooded soil. The changes in speciation determined by sequential extractions were smaller than those determined by XAS, possibly due to incomplete or nonspecific extraction (*57*). Zinc associated with organic matter and silicates, both ruled out by XAS, comprised only a minor fraction of the total Zn in the system. Some Zn was exchangeable and was not determined by XAS; however, it is unclear with which phase exchangeable Zn is associated. The similarity in Zn speciation determined by XAS and extractions indicate the utility of XAS to determine Zn partitioning in these wetlands.

Factors That Affect Zn Speciation. Many factors, including water depth (redox status), spatial and temporal variation may influence Zn speciation. The water depth and the associated redox status were used to discriminate between the different Zn phases. To test the importance of water depth on Zn speciation throughout the entire wetland, the effect of these two parameters was evaluated independent of the other environmental factors, such as spatial and seasonal variation. Zinc speciation is strongly correlated with water depth (Figure 5). In dry (oxidized) areas, nearly all Zn is sorbed on (hydr)oxides or present as a discrete ZnO phase. ZnS and $ZnCO_3$ form in response to the lowered reduction potential associated with flooding and subsequent elevated sulfide and carbonate concentrations (*55*). Under shallow water (10−50 cm water column depth), the E_h was generally near +100 mV—an intermediate, suboxic redox status. Therefore, soils under these shallow waters contained significant fractions of ZnO/sorbed and ZnS (Figure 5). At >50 cm water column depths, the soil becomes sufficiently reduced (E_h < −100 mV) and leads to the conversion of Zn to ZnS (Figure 5). Significant quantities of $ZnCO_3$ also begin to appear in soils under deeply ponded water (>60 cm depth), leading to a decrease in the ZnS fraction. Residual ZnO/sorbed also comprises up to 15% of the total Zn, even when the redox

TABLE 4. Zn Speciation Determined by Selective Sequential Extraction for Both Shallow Ponded and Flooded Wetland Sites

			mg kg^{-1}							
sample	date	water depth, cm	$MgCl_2$ (exchangeable)	acetic acid (carbonates)	AOD[a] (non-crystalline oxides)	HCl-AOD[c] (acid-volatile sulfides)	NaOCl (org matter)	HH[b] (crystalline oxides)	HF (silicates)	HNO_3 (pyritic)
shallow ponded	25 Jan	21	318 ± 31[¥d]	99 ± 9	93 ± 9	205 ± 20	97 ± 9	121 ± 12	80 ± 8	1 ± 0.1
	5 Mar	33	3 ± 0.3	30 ± 3	447 ± 46	232 ± 24	108 ± 11	115 ± 13	46 ± 5	2 ± 0.2
	13 May	39	1.3 ± 0.1	64 ± 7	435 ± 46	148 ± 16	143 ± 15	34 ± 4	113 ± 12	4 ± 0.4
	8 July	46	1.8 ± 0.1	218 ± 15	604 ± 42	172 ± 12	55 ± 4	365 ± 25	35 ± 3	1 ± 0.1
	15 Sept	0	475 ± 37	200 ± 16	100 ± 782	63 ± 5	133 ± 10	242 ± 19	65 ± 5	2 ± 0.1
flooded	25 Jan	44	198 ± 17	145 ± 12	302 ± 26	215 ± 18	136 ± 11	114 ± 10	73 ± 6	1.5 ± 0.1
	5 Mar	54	5 ± 0.4	156 ± 11	545 ± 40	245 ± 18	147 ± 11	95 ± 7	176 ± 13	2 ± 0.1
	13 May	75	9 ± 0.8	236 ± 20	352 ± 30	237 ± 20	191 ± 16	45 ± 4	118 ± 10	3 ± 0.2
	8 July	25	11 ± 0.7	334 ± 21	507 ± 32	339 ± 21	101 ± 6	254 ± 16	40 ± 3	1 ± 0.1
	15 Sept	12	0.1 ± 0.1	90 ± 5	669 ± 36	573 ± 31	236 ± 13	236 ± 13	72 ± 4	2 ± 0.1

[a] Ammonium oxalate extraction. [b] Hydroxylamine-hydrochloride extraction. [c] This AVS fraction is determined by difference between the HCl extraction and the AOD extraction. [d] All values are the average of 12 replicates ± the standard deviation.

potential decreased to −200 mV, indicating that a portion of oxidized Zn species is recalcitrant and resistant to reduction.

Spatial heterogeneity and soil depth may also influence Zn speciation in wetlands. To test these effects, duplicate soil cores were collected from several sites within the wetland, and both the 0−5 and 5−10 cm sections were examined by XAS. Little variation was observed between the duplicate cores or the two core sections, suggesting that Zn speciation is similar within a given section of the wetland (Table 3). However, cores collected at different sites did contain different Zn species, even when their water levels were similar. Despite these differences, Zn speciation was still largely determined by the redox stability of each phase: either ZnO or Zn adsorbed on (hydr)oxides comprised the majority of Zn in oxic soil cores, while ZnS or $ZnCO_3$ dominated Zn speciation in anoxic environments (Table 3). Thus, the water depth and redox status were the most important variables in determining Zn speciation in this wetland.

Four principle phases, ZnO, Zn on (hydr)oxide, $ZnCO_3$, and ZnS, were found in a seasonally flooded wetland. Under aerated conditions, Zn sorbs preferentially to (hydr)oxides. Reducing conditions, promoted by the presence of standing water, favor the formation of $ZnCO_3$ and ZnS. These phase transformations occurred readily in this environment. Thus, zinc partitioning in the environment is a dynamic, and largely reversible, process in which Zn species form in response to changing conditions. Owing to the lability of the observed Zn phases, both thermodynamic and kinetic factors need to be considered when evaluating the fate of Zn in the environment.

Acknowledgments

This research was sponsored by the U.S. Department of Energy, Office of Biological and Environmental Research, Environmental Management Science Program (Grant DE-FG07-99ER62889-A01), the Exploratory Research Program of the U.S. EPA (Grant R-825399), and Stanford University Department of Geological and Environmental Sciences. X-ray absorption spectroscopy was performed at Stanford Synchrotron Radiation Laboratory (SSRL) operated by the U.S. Department of Energy. The authors would like to thank the staff at SSRL for their assistance, as well as the three anonymous reviewers for their contributions.

Literature Cited

(1) Benjamin, M. M.; Leckie, J. O. *J. Colloid Interface Sci.* **1981**, *79*, 209.
(2) Stahl, R. S.; James, B. R. *Soil Sci. Soc. Am. J.* **1991**, *55*, 1287.
(3) Loganathan, P.; Burau, R. G. *Geochim. Cosmochim. Acta* **1973**, *37*, 1277.
(4) Zasoski, R. J.; Burau, R. G. *Soil Sci. Soc. Am. J.* **1988**, *52*, 81.
(5) Stahl, R. S.; James, B. R. *Soil Sci. Soc. Am. J.* **1991**, *55*, 1291.
(6) Kornicker, W. A.; Morse, J. W. *Geochim. Cosmochim. Acta* **1991**, *55*, 2159.
(7) Huerta-Diaz, M. A.; Tessier, A.; Carignan, R. *Appl. Geochem.* **1998**, *13*, 213.
(8) Morse, J. W. *Mar. Chem.* **1986**, *20*, 91.
(9) Zachara, J. M.; Kittrick, J. A.; Harsh, J. B. *Geochim. Cosmochim. Acta* **1988**, *52*, 2281.
(10) Zachara, J. M.; Cowan, C. E.; Resch, C. T. *Geochim. Cosmochim. Acta* **1991**, *55*, 1549.
(11) Tessier, A.; Campbell, P. G. C.; Bisson, M. *Anal. Chem.* **1979**, *51*, 844.
(12) Shuman, L. M. *Soil Sci.* **1985**, *150*, 11.
(13) Fendorf, S. E.; Sparks, D. L.; Lamble, G. M.; Kelley, M. J. *Soil Sci. Soc. Am. J.* **1994**, *58*, 1583.
(14) Henderson, C. M. B.; Cressey, G.; Redfern, S. A. T. *Radiation Phys. Chem.* **1995**, *45*, 459.
(15) Schulze, D. G.; Bertsch, P. M. *Adv. Agron.* **1995**, *55*, 1.
(16) Conradson, S. *Appl. Spectrosc.* **1998**, *52*, 252A.
(17) Hesterberg, D.; Sayers, D. E.; Zhou, W.; Plummer, G.M.; Robarge, W. P. *Environ. Sci. Technol.* **1997**, *31*, 2840.
(18) O'Day, P. A.; Carroll, S. A.; Waychunas, G. A. *Environ. Sci. Technol.* **1998**, *32*, 943.
(19) Manceau, A.; Boisset, M.-C.; Sarret, G.; Hazemann, J.-L.; Mench, M.; Cambier, P.; Prost, R. *Environ. Sci. Technol.* **1996**, *30*, 1540.
(20) La Force, M. J.; Hansel, C. M.; Fendorf, S. *Environ. Sci. Technol.* **2000**, *34*, 3937.
(21) La Force, M. J.; Hansel, C. H.; Fendorf, S. *Soil Sci. Soc. Am. J.* **2000**, *64*, 809−811.
(22) Cramer, S. P.; Tench, O.; Yocum, M.; George, G. N. *Nucl. Inst. Meth.* **88**, 586.
(23) Zabinsky, S. I.; Rehr, J. J.; Ankudinov, A.; Albers, R. C.; Eller, M. J. *Phys. Rev. B* **1995**, *52*, 2995.
(24) Rehr, J. J.; Muestre de Leon, J.; Zabinsky, S. I.; Albers, R. C. *Phys. Rev. B* **1991**, B*44*, 4146.
(25) Reddy, M. M.; Nancollas, G. H. *J. Colloid Interface Sci.* **1971**, *36*, 166−172.
(26) Xia, K.; Bleam, W.; Helmke, P. A. *Geochim. Cosmochim. Acta* **1997**, *61*, 2223.
(27) Salt, D. E.; Prince, R. C.; Baker, A. J. M.; Raskin, I.; Pickering, I. J. *Environ. Sci. Technol.* **1999**, *33*, 713.
(28) Abrahams, S. C.; Bernstein, J. L. *Acta Crystallogr. B* **1969**, *25*, 1233.
(29) Hang, C.; Simonov, M. A.; Belov, N. V. *Krystallographiya* **1970**, *15*, 457.
(30) Ghose, S. *Acta Crstallogr.* **1964**, *17*, 1051.
(31) Koenig, V.; Chol, G. *J. Appl. Crystallogr.* **1968**, *1*, 124.
(32) Kisi, E. H.; Elcombe, M. M. *Acta Crystallogr. C* **1989**, *45*, 1867.
(33) Lee, F. Y.; Kittrick, J. A. *Soil Sci. Am. J.* **1984**, *48*, 548.
(34) Clark-Baldwin, K.; Tierney, D. L.; Govindaswamy, N.; Gruff, E. S.; Kim, C.; Berg, J.; Koch, S. A.; Penner-Hahn, J. E. *J. Am. Chem. Soc.* **1998**, *120*, 8401.
(35) Hansel, C. M.; La Force, M. J.; Sutton, S. E.; Fendorf, S. 2001. In *Crerar Volume*; Wood, S., Hellmann, R., Eds.; Geochemical Society Special Publication, Geochemical Society of America; St. Louis, in press.
(36) Morra, M. J.; Fendorf, S. E.; Brown, P. D. *Geochim. Cosmochim. Acta* **1997**, *61*, 683.
(37) Xia, K.; Weesner, F.; Bleam, W. F.; Bloom P. R.; Skyllberg, U. L.; Helmke, P. A. Soil *Sci. Soc. Am. J.* **1998**, *62*, 1240.
(38) Christiansen, A. N. *Acta Chim. Scand.* **1969**, *23*, 2016.
(39) Effenberger, H.; Mereiter, K.; Zemann, J. *Z. Kristallogr.* **1981**, *156*, 233.
(40) Reeder, R. J.; Lamble, G. M.; Northrup, P. A. *Am. Mineral.* **1999**, *84*, 1049.
(41) Papadopoulos, P.; Rowell, D. L. *J. Soil Sci.* **1989**, *40*, 39.
(42) Boyanov, B. I.; Bunker, G.; Morrison, T. I. *J. Synchrotron Radiation* **1996**, *3*, 120.
(43) Nishi, K.; Shimizu, K.; Takamatsu, M.; Yoshida, H.; Satsuma, A.; Tanaka, T.; Yoshida, S.; Hattori, T. *J. Phys. Chem B* **1998**, *102*, 10190.
(44) Ressler, T.; Wong, J.; Roos, J.; Smith I. L. *Environ. Sci. Technol.* **2000**, *34*, 950.
(45) Foster, A. L.; Brown, G. E., Jr.; Tingle, T. N.; Parks, G. A. *Am. Mineral.* **1998**, *83*, 553.
(46) Engler, R. M.; Patrick, W. H., Jr. *Soil Sci.* **1975**, *119*, 217.
(47) Simpson, S. L.; Apte, S. C.; Batley, G. E. *Environ. Sci. Technol.* **2000**, *34*, 4533.
(48) Carroll, S. A.; O'Day, P. A.; Waychunas, G. A. *Environ. Sci. Technol.* **1998**, *32*, 956.
(49) Masscheleyn, P. H.; Pardue, J. H.; DeLaune, R. D.; Patrick, W. H., Jr. *Environ. Sci. Technol.* **1992**, *26*, 1217.
(50) Tokunaga, T. K.; Pickering, I. J.; Brown, G. E., Jr. *Soil Sci. Soc. Am. J.* **1996**, *60*, 781.
(51) Matsunaga, T.; Karametaxas, G.; Von Gunten, H. R.; Lichtner, P. C. *Geochim. Cosmochim. Acta* **1993**, *57*, 1691.
(52) Thamdrup, B.; Glud, R. N.; Hansen, J. W. *Geochim. Cosmochim. Acta* **1994**, *58*, 2563.
(53) Farley, K. J.; Dzombak, D. A.; Morel, F. M. M. *J. Colloid Interface Sci.* **1985**, *106*, 226.
(54) Prieto, M.; Fernandez-Gonzalez, A.; Putnis, A.; Fernandez-Diaz, L. *Geochim. Cosmochim. Acta* **1997**, *61*, 3383.
(55) Stumm, W.; Morgan, J. J. *Aquatic Chemistry*, 3rd ed.; John Wiley and Sons: New York, 1996; p 1022.
(56) Belzile, N.; Lecompte, P.; Tessier, A. *Environ. Sci. Technol.* **1989**, *23*, 1015.
(57) Davidson, C. M.; Thomas, R. P.; McVey, S. E.; Perala, R.; Littlejohn, D.; Ure, A. M. *Anal. Chim. Acta* **1994**, *291*, 277.
(58) Cooper, D. C.; Morse, J. W. *Environ. Sci. Technol.* **1998**, *32*, 1076.

Received for review January 18, 2001. Revised manuscript received June 9, 2001. Accepted June 12, 2001.

ES010549D